Appl. Phys. B 69, 137–146 (1999) / Digital Object Identifier (DOI) 10.1007/s003409900015

Applied Physics B
Lasers
and Optics

A pulse-pileup correction procedure for rapid measurements of hydroxyl concentrations using picosecond time-resolved laser-induced fluorescence

M.W. Renfro*, S.D. Pack, G.B. King, N.M. Laurendeau**

Flame Diagnostics Laboratory, School of Mechanical Engineering, Purdue University, West Lafayette, IN 47907-1288, USA

Received: 9 October 1998/Revised version: 30 December 1998/Published online: 28 April 1999

Abstract. The measurement of fluorescence lifetimes is important for determining minor-species concentrations in flames when using linear laser-induced fluorescence (LIF). Applications of LIF to turbulent flames require that the quenching rate coefficient be determined in less than ~ 100 μs. Moreover, the measurement technique must be insensitive to the existence of relatively large backgrounds, such as occur from flame emission. To meet these goals, we have recently developed a rapid, gated photon-counting technique, termed LIFTIME. However, for ultimate application to turbulent time-series measurements, LIFTIME must be extended to photon count rates which unfortunately result in nonlinear discriminator operation. In this paper, a correction technique is derived to permit quantitative measurements of fluorescence lifetimes and concentrations at sampling rates up to 4 kHz. The technique was tested against liquid samples having a known lifetime and is further shown to reproduce previous hydroxyl concentration measurements in a series of laminar flames with total photon count rates of up to ~ 35 million detected photoelectrons per second. The fluorescence lifetimes and hydroxyl concentrations are shown to be measured with $\sim 10\%$ accuracy (68% confidence interval) for sampling times as low as 250 μs.

PACS: 82.40; 34.50; 02.50

The study of turbulent reacting flows requires quantitative determination of both scalar and velocity fields. For many applications, it is only the mean fields which are of immediate importance for determining global quantities such as total pollutant emissions or the total heat transfer rate. However, in an attempt to provide more accurate predictions, the temporal behavior of the scalar and vector fields provides yet another constraint for turbulent combustion modeling. Moreover, time-resolved scalar measurements can provide information on the interactions between turbulence and chemical reaction which may be difficult to resolve from time-averaged data. A detailed understanding of these effects is important to providing better models and, hence, better combustor designs.

The study of radical concentration spectra could provide a means for direct investigation of turbulence-chemistry interactions and would supplement existing time-resolved measurements for velocity [1–3] and for other scalars [4–8]. However, quantitative time-series measurements of minor-species concentrations are not trivial and have not yet been presented in the literature. Recently CH- and OH-fluorescence time series were obtained for the first time [9, 10], but these measurements were not corrected for electronic-quenching dependencies.

Our present research focuses on new measurements of OH concentration by using picosecond time-resolved laser-induced fluorescence (PITLIF) combined with on-the-fly quenching corrections. These on-the-fly lifetime measurements are made using a gated, photon-counting system, termed the laser-induced fluorescence triple-integration method (LIFTIME), which was recently developed by Pack et al. [11]. This system was tested against liquid samples of known lifetime and was later applied successfully to hydroxyl measurements in laminar flames [12]. The measurements were limited to sampling rates of 500 Hz, and thus to laminar flames, owing to the need to attenuate the fluorescence signal below that level for which pulse pileup becomes important. For these low signals, the response of the photon-counting system was linear; however, shot noise limited the maximum frequency resolution.

Several researchers have examined the efficacy of numerically correcting data which violates the upper limit for unsaturated photon counting. Coates [13] derived a formula for correcting each successive bin of time-correlated, single-photon counting (SPC) data based on the laser repetition rate and previous bin counts. However, this formula only explicitly applies to SPC data, i.e., data taken with a time-amplitude converter (TAC), and does not work if the source irradiance is fluctuating [14]. Donohue and Stern [15] also derived a correction technique for saturated data and demonstrated the improved efficiency of SPC measurements at higher photon count rates. In their numerical simulations, the authors found

* Corresponding author. Fax: +1-765/494-0539, E-mail: renfro@ecn.purdue.edu

** *Present address*: Rolls Royce-Allison Engine Company, Plant 8 Mailroom, 2001 South Tibbs Avenue T14, Indianapolis, IN 46241-4812, USA

that the optimum photon detection rate for their correction scheme corresponded to an average of one photon per laser pulse.

Gated photon-counting techniques share many similarities to time-correlated SPC in that the sparse photon counts are distributed into bins which build up the fluorescence decay. The primary difference is the lack of a TAC, which is the main count-rate limitation in traditional SPC measurements [16]. Unlike SPC, gated photon-counting is not limited to only one collected photon per laser pulse and is not affected by the same pulse pileup statistics. Since the saturation behavior for gated photon-counting differs from that for SPC, the total data rate can be increased significantly [17]. As with SPC methods, the data must generally be deconvolved from the instrument response function [18]; however, it is not feasible to make deconvolution computations for the large amount of data that is inherent to time-series measurements.

In this paper, a saturation correction procedure is derived which is applicable to the gated photon-counting measurements characteristic of LIFTIME [11]. This routine is shown to provide fluorescence decay amplitudes, lifetimes, and backgrounds at data collection rates up to 35 million photoelectrons per second. For our Ti:sapphire laser system, this represents an average of almost one detected photon per two laser pulses and approaches the optimal data rate of Donohue and Stern [15]. The correction was calibrated and tested against liquid solutions with known fluorescence lifetimes. Using the correction algorithm at high signal levels, the measurements of Pack et al. [12] were then repeated in a series of laminar premixed and counterflow diffusion flames. The measurements are shown to agree with the previous low-signal results in each case. Measurements were also made in a laminar, methane/air nonpremixed jet flame at sampling rates of up to 4 kHz. This data rate is fast enough for eventual application to turbulent flames. The results of these measurements are used to discuss the implications for turbulent time-series measurements.

1 Experimental apparatus

A diagram of the laser system including the burner station is shown in Fig. 1. The Spectra Physics Tsunami, regeneratively mode-locked, Ti:sapphire laser was pumped by a 20-W, Spectra Physics argon-ion, multi-mode laser. After leaving the Tsunami, the IR beam was frequency tripled to ~ 309 nm in a CSK SuperTripler. The resulting beam was recollimated by two UV lenses and focused by a 22.9-cm-focal-length, 5.1-cm-diameter UV lens through the probe volume above the burner assembly. The laser beam was then dumped into a radiometer which recorded the average laser power. This power measurement was used to scale much of the reported mean data to correct for long-term laser power fluctuations; however, since measurements from the radiometer cannot be easily correlated to measurements via the photon-counting boards, the high repetition rate measurements were not corrected for fluctuations in laser power. Fortunately, no substantial short-term fluctuations in laser power were observed with the Tsunami system. For the tripled beam, the beam diameter (e^{-2}) was measured at the probe volume to be ~ 71 μm in two perpendicular directions. The laser power was approximately 18–24 mW which resulted in an average probe volume irradiance of $\sim 3.5 \times 10^5$ mW/cm^2. The $Q_1(8)$ transition of the (0,0) vibronic band (309.33 nm) was chosen for excitation. This line displays an approximately ±5% Boltzmann fraction variation over the temperature range 1500–2250 K.

The hydroxyl fluorescence was collected at a 90° angle from the incident laser beam by two 14.1-cm-focal-length, 10.2-cm-diameter UV lenses with a magnification of 4.1. This allowed collection of approximately 1/15 of all fluorescence photons emitted from the probe volume. For many of the premixed flame measurements, a mask on the primary detection lens was used to avoid fluorescence vignetting from the burner surface which decreased the solid collection angle. This masking was not necessary for the methane jet flame. The wavelength of the measured fluorescence was selected by use of a 0.25-m monochromator. An adjustable slit at the entrance to the monochromator allowed the probe volume in the flame to be limited along the beam path. The beam diameter itself defines the other two probe-volume dimensions, although black tape on the monochromator was used to limit some flame emission in the axial direction. These probe-volume settings were varied throughout the measurements to control the total signal level and are reported with the data. For most measurements the spectral window was set at a total

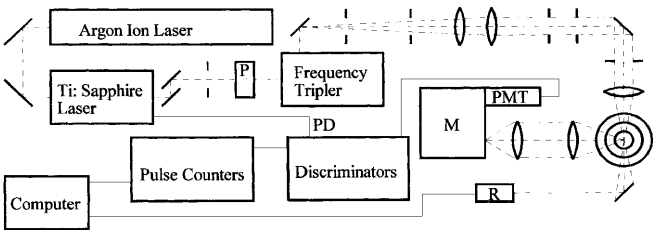

Fig. 1. Experimental setup for the laser system: P, polarization rotator; M, 0.25-m monochromator; P, radiometer; PD, photodiode trigger from the laser to the discriminators

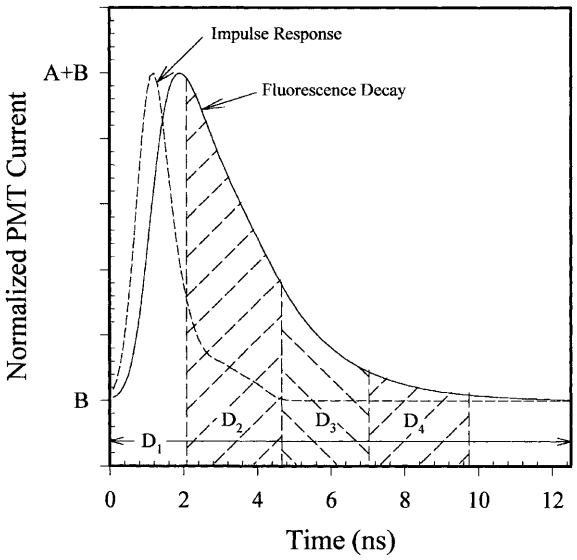

Fig. 2. PMT impulse response function as compared to a typical fluorescence decay. The areas D_2, D_3, and D_4 represent the integrated measurements of the gated photon counting system. D_1 represents the total integrated fluorescence signal (ungated). The background, B, is typical of flame emission, and the amplitude, A, is proportional to concentration

bandwidth of 10 nm, centered at 309 nm. A Hamamatsu HS5321 PMT detected the fluorescence at the exit plane of the monochromator. The PMT was biased at −2500 V to increase the single-photon pulse height for subsequent leading-edge discrimination. This PMT has a risetime of 700 ps and a transit time spread of 160 ps. The PMT impulse response function (∼ 1 ns FWHM) is shown in Fig. 2 and is compared to a typical fluorescence decay. The three areas D_2, D_3, and D_4 represent the three measurements of the gated, photon-counting system. The other measurement, D_1, represents the total integrated fluorescence signal. The method for computing the decay lifetime from these bins will be discussed in the next section.

The wire schematic for the gated, photon-counting system is provided by Pack et al. [11]. Briefly, the system consists of two LeCroy model 4608C, eight-channel discriminators connected to four EG&G Ortec logic-pulse counting boards. The four photon-counting boards each have an 8192 channel memory and can be sampled simultaneously. Each channel acquires counts over many thousands of laser pulses as set in software. The maximum sampling rate (channel advance rate) for the boards is 500 kHz, well above that needed for turbulence studies. Further details of the PITLIF/LIFTIME gated, photon-counting system are available from Pack et al. [11].

2 Correction for photon saturation

In this section, we characterize the nonlinear behavior of the photon-counting system. As an extension of the linear work of Pack et al. [12], a pulse-pileup correction procedure is detailed leading to the presentation of a complete PITLIF instrument capable of quantitative time-series measurements at signal levels up to the point of PMT saturation and at sampling rates up to 4 kHz.

2.1 Equipment characterization

Upon receiving an analog pulse which meets the threshold criterion, the discriminator begins to output a NIM logic pulse (0 to −0.8 V, typically less than 5 ns duration, with ∼ 1 ns rise and fall times). However, if a second acceptable analog pulse arrives during the time required to complete the NIM pulse output, the discriminator is unable to respond (or is dead) and the measured count rate will be lower than the actual incoming pulse rate. For the LeCroy discriminators, the minimum dual-pulse resolution (DPR) is 4.5 ns based on the manufacturer's specifications. However, since the output pulse rate is directly related to (although not linear with) the input pulse rate, a one-to-one relationship can be derived such that the measured output rate can be used to infer the actual input rate.

Figure 3 shows a measurement of the discriminator saturation or pulse pileup for our photon-counting system. For this measurement, a flashlight was placed at the probe volume and a neutral-density filter wheel was placed before the monochromator to change the absolute signal level. As observed, the measured counts are not linear with signal, and the percentage undercount increases with signal level. The counts for the three gated channels (D_2, D_3, and D_4) in Fig. 3 are scaled by the gate duty cycle ($\Delta t/12.5$ ns, where

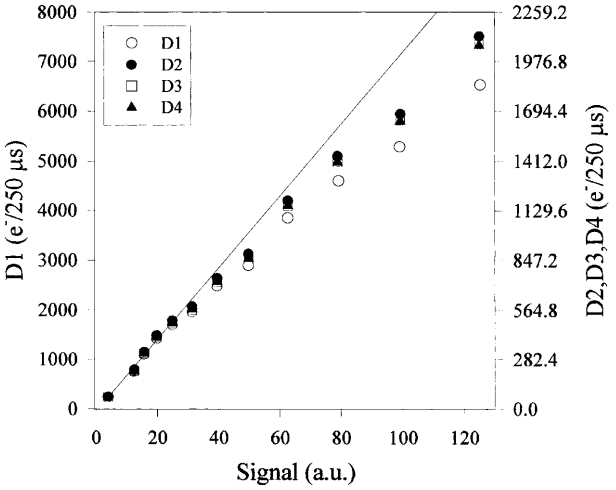

Fig. 3. Measured photon count rates for the ungated board, D_1, and for each of the gated boards, D_2–D_4. The secondary y axis is scaled by the gate duty cycle (3.53/12.5 in this case) such that the gated counts can be visually compared to D_1. The photon source was a flashlight at the probe volume. The *straight line* is a linear extrapolation of low signal (non-saturated) measurements

$\Delta t = 3.53$ ns is the gate width) such that they should measure the same number of counts as the ungated channel D_1. A discrepancy is apparent as the scaled count rates for the gated channels seem to be systematically higher than that for the ungated channel. This discrepancy arises from secondary pulse pileup at the EG&G enumerators which are characterized by their own DPR (> 5 ns). Since the width of each gated bin is less than that of a typical NIM pulse, the gated channels are not susceptible to this secondary saturation. This was verified by inserting a prescaler between the D_1 discriminator output and the pulse counting board. The prescaler was set to provide one pulse for every 2048 input pulses. In this way, all potential saturation at the photon counting board was removed. This measurement is shown in Fig. 4. Both the gated

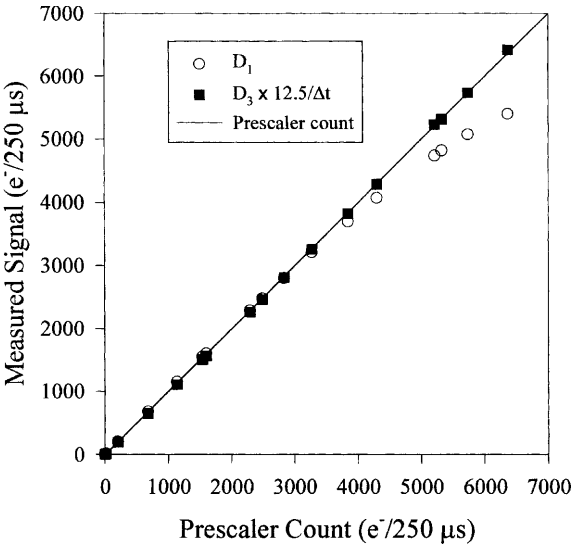

Fig. 4. Comparison of gated and ungated board counts to the counts from a prescaler. The prescaler is placed between the D_1 discriminator and the pulse counting board

count for channel D_3 (scaled by the gate duty cycle) and the ungated count (prior to the prescaler) are plotted versus the prescaler count (multiplied by 2048). The gated count is observed to be almost exactly linear with the prescaled count while the ungated count is partially saturated.

Another discrepancy which is apparent in Fig. 3 is the small count differences from one gated channel to the next. This was noted by Pack et al. [11] and was attributed to small inherent differences in each discriminator channel. In particular, these differences could be caused by small variations in the NIM-pulse height from one channel to the next or by the effectiveness or timing of the gate pulse. Pack et al. [11] account for these differences by daily calibrations using a flashlight at the probe volume. The bins are corrected such that each provides the same count for the flashlight measurement. Typically, the corrections are 2%–3% for bins D_3 and D_4 (scaled to match D_2). The correction factors are weak functions of ambient temperature and appear to be very stable ($< 0.5\%$ variation) over the course of many days. This channel-to-channel correction was made to all of the data considered here.

2.2 Saturate-and-compare procedure

The next step in the data analysis is to determine the lifetime, background, and peak decay amplitude from the measured counts, D_2–D_4. For the unsaturated case, this is a simple algebraic calculation as derived in detail by Pack [19]. Summarizing the results:

$$\tau = \frac{\Delta t}{\ln\left[\frac{D_2 - D_3}{D_3 - D_4}\right]}\,, \tag{1}$$

$$C \equiv \exp\left(\frac{-\Delta t}{\tau}\right) = \frac{D_3 - D_4}{D_2 - D_3}\,, \tag{2}$$

$$B = \frac{C^2 D_2 - D_4}{(C^2 - 1)\Delta t}\,, \tag{3}$$

$$A = \frac{D_2 - B\Delta t}{(1 - C)\tau}\,, \tag{4}$$

where τ is the fluorescence lifetime, B is the constant background, A is the initial decay amplitude at the start of D_2, and C is defined for convenience. This calculation is easily accomplished "on-the-fly" for time-series measurements. However, the algebraic solution was derived assuming a pure-exponential, single-lifetime decay with constant background (uncorrelated with the laser pulse) and negligible instrumentation effects. These assumptions do not hold once the measurements are affected by nonlinear pulse pileup. Fortunately, the saturation process is fairly well understood given that the DPR is known, and pulse-pileup corrections have been shown to be effective [15, 16, 20].

An iterative routine, termed "saturate-and-compare", was derived to account for pulse pileup. This approach is similar to convolute-and-compare routines which are commonly used to account for instrumentation response functions in accurate determinations of fluorescence lifetimes. The procedure here is as follows: (i) assume values for the decay parameters (τ, B, and A), (ii) simulate a perfect exponential decay, (iii) saturate the decay based on the observed behavior of our system, (iv) compute the simulated bin counts, D_2–D_4, and (v) compare the simulated and measured counts to improve the decay parameters, eventually converging to the correct values. The mechanics of this calculation and the accompanying saturation model are briefly presented in Appendix A. The saturate-and-compare model depends on the system DPR and the temporal delay (t_o) between the laser pulse and the first gated bin, D_2. The calibration of the model to determine these parameters is addressed in Appendix B. A FORTRAN version of the resulting saturate-and-compare code, which is used for all the measurements of this investigation, is available via the Internet [21].

3 Results

3.1 Liquid solutions

As verification of the capabilities of saturate-and-compare, measurements were taken of diphenyloxazole (PPO) and each of six quinine sulfate monohydrate (QSM) solutions [11]. The PPO solution has a known lifetime of 1.28 ns [22] and the QSM solutions have lifetimes that can be controlled by changing the salt concentration in the solvent [23]. The lifetime of each of these solutions has been measured using an existing convolute-and-compare technique which has been shown to yield accurate results [19]. A calibration plot of the saturate-and-compare results as compared to the known values is shown in Fig. 5. The experimental lifetimes are almost identical to the low-signal LIFTIME results of Pack et al. [11]. Thus, the saturate-and-compare routine is providing the correct average lifetime from 1.3 to 3.0 ns. The error bars in Fig. 5 show the standard deviation measured over a full range of signal levels and signal-to-background ratios (SBR $= D_2/D_4 - 1$). The relatively small size of the error

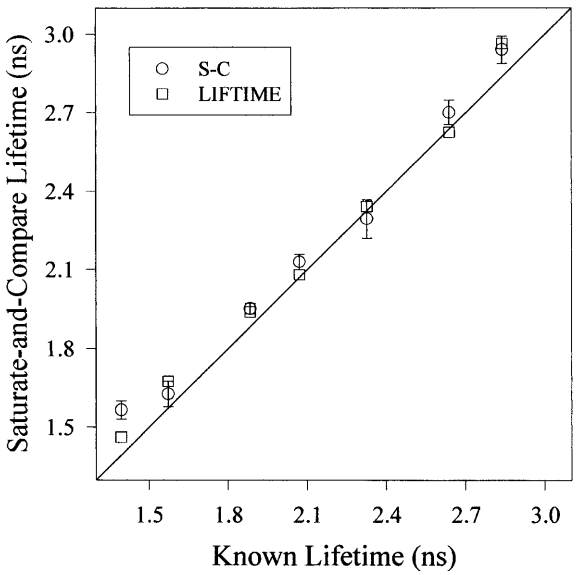

Fig. 5. Calibration plot of saturate-and-compare (S-C) lifetimes as compared to the known convolute-and-compare measurements of Pack et al. [11]. *Error bars* represent the standard deviation (68% confidence interval) for measurements at many different signal levels and SBRs. The LIFTIME measurements from Pack et al. [11] represent the exact solution to (1) at low signal levels

bars indicates that the system can converge to the correct solution over all of the expected input conditions.

As discussed in Appendix A, the measured bin, D_1, was not used in the saturate-and-compare algorithm. However, D_1 can be computed from the saturate-and-compare routine and thus compared to its measured value as a check for the routine. In making this comparison, careful consideration must be given to the effect of secondary saturation at the counters. The resulting comparison of the measured and the predicted D_1 is shown in Fig. 6 for all of the PPO and QSM data used in Fig. 5. The comparison is remarkably good considering that D_1 was not used for the optimization of DPR and t_o in the saturation model (Appendix B). In particular, this agreement confirms that the choice of t_o is reasonable as the predicted D_1 is very sensitive to this temporal delay parameter. Since the initial delay is accurately determined, the peak decay amplitude predicted by saturate-and-compare, A, represents the fluorescence signal just after impulse laser excitation. This initial signal is independent of quenching and can be taken to be proportional to concentration, as observed from the governing rate equations [24]. This feature has been experimentally justified via measurements in a counterflow diffusion flame (discussed subsequently). Except where noted, all of the hydroxyl concentrations in this investigation were taken as directly proportional to the modeled value of A.

The performance of the saturate-and-compare algorithm is most important at high signal levels, since time-series measurements would then be permitted at higher sampling rates. Pack et al. [11] showed that the photon counting system was capable of resolving fluorescence lifetimes to within ±10% up to a sampling rate of 500 Hz without saturation effects. This limit was determined by measuring PPO lifetimes at various signal levels up to the saturation point (∼ 1 million photoelectrons/second). The four signal levels of Pack et al. [11] are reproduced in Fig. 7 along with our results at four higher signal levels. These new data were taken in the saturation regime and utilized the saturate-and-compare correction. As observed, the power-law trend in error versus sampling rate is maintained for both the LIFTIME and saturate-and-compare calculations. Furthermore, the lifetime uncertainty decreases with increasing signal, consistent with the previous measurements. At the highest signal level considered (∼ 33 million photoelectrons/second, close to the PMT saturation point) the lifetime error is below 10% up to 7.8 kHz. This is approximately double the sampling rate that was used in our previous PITLIF measurements [9, 10] and is a considerable improvement over the previous 500-Hz limit for unsaturated photon counting [11].

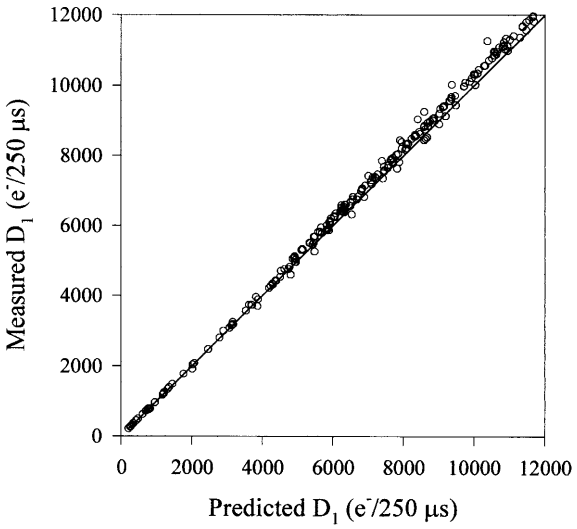

Fig. 6. Measured D_1 corrected for secondary saturation as per the observed relationship of Fig. 4. This corrected value is plotted versus the predicted D_1 from the saturate-and-compare algorithm

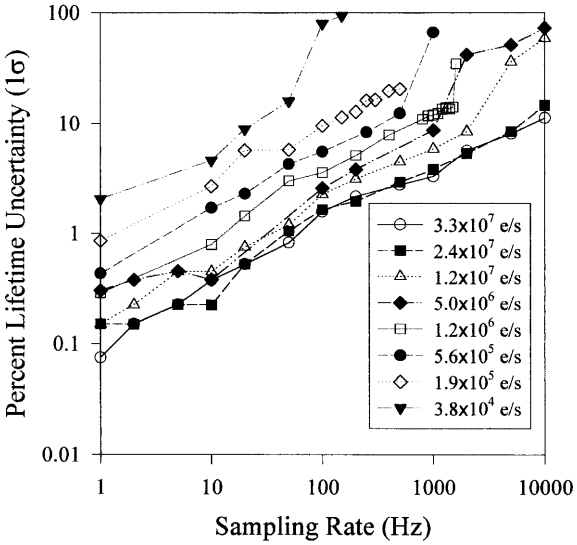

Fig. 7. Lifetime uncertainty (68% confidence interval, 100 samples) as a function of sampling rate. Each curve represents a different signal level as determined from the total photon count (D_1). The lifetimes for the four highest signals are affected by saturation and are computed from saturate-and-compare. The lifetimes for the four smallest signals are from Pack et al. [11] and are computed from (1)

3.2 Hydroxyl measurements in laminar premixed flames

Since the ultimate goal of the PITLIF technique is to provide concentration time series, the effects of experimental and numerical uncertainty on measured concentrations is of more direct importance than the effects on lifetimes. Moreover, the absence of a background in liquid solutions does not adequately simulate actual conditions that are encountered in hydroxyl measurements. Hence, to further verify our pulse-pileup correction procedure, measurements of OH concentration were taken in a 0.8-equivalence ratio, 3.1-dilution ratio ($[N_2]/[O_2]$), $CH_4/N_2/O_2$ laminar premixed flame. For these measurements, the spatial resolution along the laser beam was chosen to be 250 μm.

Sampling rate measurements similar to those shown in Fig. 7 were made with a SBR of 2.6 at 3 mm above the burner. The uncertainty in lifetime was very similar to that of PPO. However, the sampling rate at which the peak amplitude (or concentration) reached an error of ±10% was only 3.4 kHz, which is still a significant improvement over previous unsaturated work but unfortunately much less than that for the fluorescence lifetime. This is not unexpected, however, as the concentration requires indirect corrections for both the background and lifetime and thus involves more usage of shot-noise-limited bin counts.

Although the uncertainty in both fluorescence lifetime and peak amplitude rises at higher sampling rates owing to reduced photon counts in each bin, the average values of the three decay parameters do not change significantly with changes in sampling rate. A small amplitude bias error exists at the highest sampling rate (10 kHz) owing to points in the time series which do not converge (for which A is set to zero). To avoid these bias errors, the maximum sampling rate for a particular measurement location should not exceed that for which the saturate-and-compare algorithm always converges; here, this cutoff sampling rate is around 5 kHz.

Figure 8 shows the average lifetime and concentration computed at a sampling rate of 5 kHz for various signal levels at a height of 3 mm in the methane premixed flame. The measured concentration is scaled by the total signal level at each point such that it should be constant in the absence of saturation. Using the saturate-and-compare algorithm, the same lifetime (within $\pm 0.5\%$) and concentration (within $\pm 2.6\%$) is recovered regardless of the degree of saturation. For comparison, these same parameters were computed using the method described by Pack et al. [12] which does not consider saturation. The need for the saturation correction is very apparent as the resulting error in lifetime exceeds 30% at the highest signal level resulting in a 20% bias error in the computed concentration. The slight curvature that exists in the corrected lifetimes and concentrations as a function of fluorescence signal most likely arises from the change in SBR as the monochromator slit is opened and closed for this measurement. This curvature would be amplified if there were any errors in the constants which are used to correct for counting variations in the discriminators. However, for each of the measurements reported here, the variation in average lifetime is always less than 2% for any one point in a flame over the full range of signal levels.

The low-signal measurements of Pack et al. [12] in a series of laminar, premixed ethane flames were shown to yield excellent agreement with modeling and with laser-saturated fluorescence results from previous studies [25]. As further verification of the saturate-and-compare algorithm's accuracy, many of these previous measurements were repeated at high signal levels. Figure 9 shows axial profiles of OH concentration in these laminar, premixed, $C_2H_6/N_2/O_2$ flames. The dilution ratio for each flame was 3.1 and the equivalence ratio was varied from 0.6 to 1.6. All measurements were taken with a spatial resolution of $\sim 250\,\mu$m along the laser beam. The peak signal corresponded to ~ 24 million photoelectrons/second. At the lowest heights in the flames of higher concentrations, there was substantial fluorescence trapping. The concentration at these heights was taken from the peak concentration displayed by radial profiles at each height. For the ($\Phi = 0.6$, 0.8, and 1.0 flames, these low-height measurements were made at radial locations within a few mm of the edge of the burner. However, for each flame, the concentrations above 6 mm were measured as close to the center of the burner as possible with the present detection optics.

Each flame in Fig. 9 was calibrated against the 6-mm measurement in the 0.8-equivalence ratio flame. The concentration at this point was set equal to that predicted by the Sandia PREMIX flame code [26] using GRIMech version 2.11 [27]. Such modeling results were found previously to be in very good agreement with the LSF measurements of Reisel et al. [25] for lean to slightly rich conditions ($0.6 < \Phi < 1.2$). In addition to the present measurements, the previous LSF measurements are shown for comparison. The agreement is excellent for nearly all cases. In particular, the PITLIF measurements resolve each of the peak locations and concentrations with high accuracy. The exception is the $\Phi = 0.8$ flame for which the peak measured concentration is $\sim 10\%$ high. To

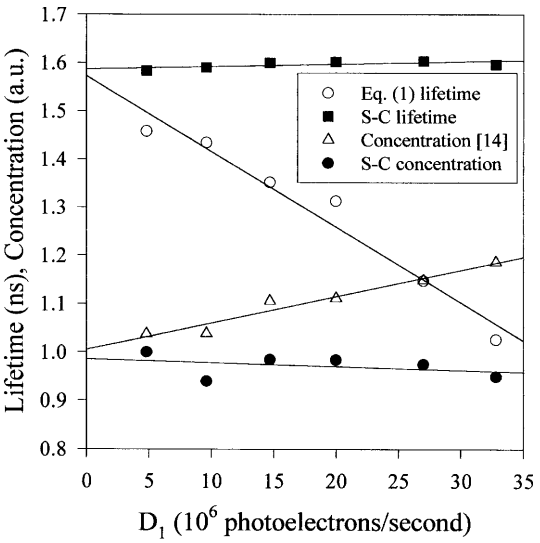

Fig. 8. Lifetime and concentration versus signal (D_1) for measurements in a laminar premixed methane flame ($\Phi = 0.8$, $\Psi = 3.1$, $z = 3$ mm). The sampling rate is 5 kHz. The signal is varied by adjusting the monochromator entrance slit. The solution obtained via the saturate-and-compare (S-C algorithm is compared with that obtained by neglecting saturation, using (1) and the technique of Pack et al. [12]. For both methods, the measured concentration is scaled by the total signal such that the results should be constant in the absence of saturation

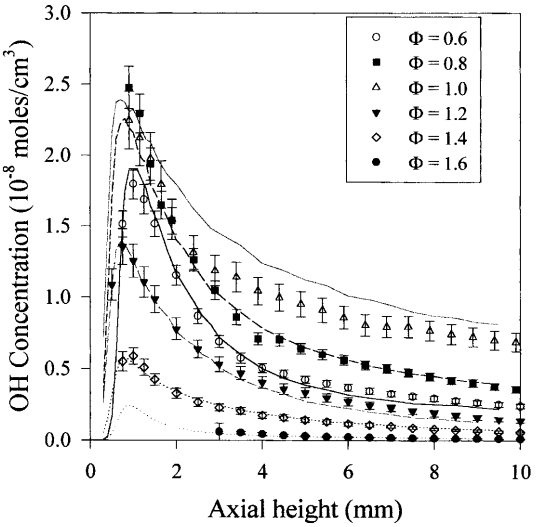

Fig. 9. Measurements of OH concentration in six premixed ethane flames. The *curves* are the LSF data of Reisel et al. [25]. All measurements are calibrated to that at an axial height of 6 mm in the $\Phi = 0.8$ flame. Each point is the average of 10 measurements taken at a sampling rate of 10 Hz. The *error bars* represent the total accuracy (95% confidence interval) and include shot-noise, flow-rate errors (3.8%–7.8%, depending on the stoichiometry), calibration errors (3.8%), and errors arising from fluctuations in the laboratory temperature (2.2%, as they affect the discriminators and thus the lifetime measurements, Pack et al. [12])

avoid fluorescence trapping, the two highest concentrations measured for the $\Phi = 0.8$ flame had to be made at a radial location 0.5–1 mm closer to the edge of the burner than for any other measurement. The discrepancy between these measured points and the previous LSF results is likely a result of entrainment at the flame edge. Another difference in the PITLIF and LSF results is apparent for the stoichiometric flame for which the present concentrations are lower than previously measured by Reisel et al. [25]. These differences might be explained by slight errors in the gas flow rates, although similar differences were observed by Pack et al. [12].

The richest flame studied ($\Phi = 1.6$) shows very good agreement between the two measured concentration profiles; however, concentrations could not be determined below ~ 3 mm. This flame was very unsteady, and the SBR for the lower heights was often below 0.1. This SBR is apparently not accessible with the PITLIF/saturate-and-compare method, although this is a minor limitation for most flame studies.

3.3 Hydroxyl measurements in laminar diffusion flames

Measurements of hydroxyl concentration in a counterflow methane/air diffusion flame (25% fuel-side nitrogen dilution, overall flame stretch rate $= 19.1\ s^{-1}$) are shown in Fig. 10. The burner was identical to that used by Ravikrishna and Laurendeau [28] for NO measurements and the flow conditions are identical to those used by Pack et al. [12] for OH measurements. As observed in Fig. 10, the present measurements, at a peak signal of 26 million photoelectrons/second and a sampling rate of 1 Hz, agree very well with the low-signal measurements from the previous work.

Three data sets are shown for the saturation-corrected data in Fig. 10. One data set is computed from D_1 plus the measured background and lifetime, as $[\mathrm{OH}] \propto (D_1 - B)/\tau$ [12]. The other two curves are simply the amplitude, A, as determined from the saturation-and-compare routine. As observed, there is no discernable difference among the three evaluations of the hydroxyl concentration. This is expected from the rate equations governing the linear fluorescence technique [24]. Hence, for all of the measurements in the present work, the concentration was determined directly from the amplitude to avoid the necessity of secondary-saturation corrections to D_1 and thus further post-processing. Although the agreement in Fig. 10 is excellent with respect to the low-signal concentration measurements of Pack et al. [12], there is an $\sim 3\%$ difference in the measured lifetimes. This could arise from flowrate errors or could be the result of partial saturation in the previous LIFTIME measurements.

The final measurements of this study were obtained in a buoyant, laminar methane jet diffusion flame ($\mathrm{Re} = 70$, burner diameter $= 5.5$ mm). This flame was previously studied using PITLIF by Renfro et al. [9, 10]; however, the effects of quenching fluctuations were not considered. Figure 11 shows a radial profile of both the OH concentration and lifetime in this flame at an axial height of 5 mm. Since this flame had a strong 15-Hz frequency corresponding to buoyancy-induced pulsations, the sampling rate for this measurement was extended to 100 Hz to avoid errors in the average lifetime measurements. As a test of the system's capability at even higher sampling rates, these measurements were also repeated at 4 kHz, a sampling rate that has been used in our previous turbulent time-series measurements [9, 10]. At the location of peak concentration, the concentration accuracy is $\pm 10.4\%$ including the uncertainties arising from calibration, which was performed with respect to a 0.8-equivalence

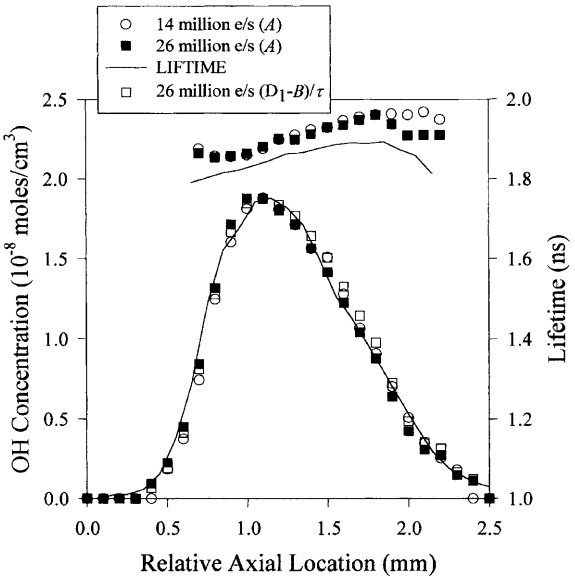

Fig. 10. Comparison of hydroxyl measurements in a counterflow diffusion flame at high signal to those of Pack et al. [12] at low signal (LIFTIME measurements). The sampling rate for these measurements was 1 Hz. Two signal levels are shown for the saturate-and-compare measurements. For the higher signal case, the concentration is computed both from the amplitude, A, and from D_1 (plus B and τ) for comparison. The spatial resolution for this measurement is ~ 1 mm along the laser beam

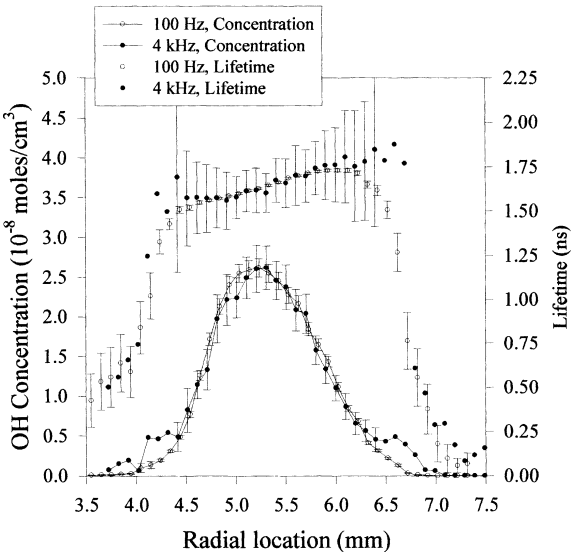

Fig. 11. Measurements of OH concentration in a buoyant, laminar methane jet diffusion flame. The burner centerline is at zero mm. The spatial resolution is < 100 μm along the laser beam and the peak signal represents ~ 32 million photoelectrons/second. Each concentration is calibrated to a $\Phi = 0.8$, methane premixed flame ($z = 8$ mm, $[\mathrm{OH}] = 5.7 \times 10^{-9}$ moles/cm^3) as detailed by Pack et al. [12]. The concentration error bars include repeatability, plus temperature and calibration errors as in Fig. 9, whereas the lifetime *error bars* consider only repeatability. For the 100 Hz measurements and one second of averaging time, the error bars represent the 95% confidence interval of the mean. For the 4 kHz measurements, the *error bars* represent the 68% confidence interval for single-point measurements

ratio, $CH_4/N_2/O_2$, premixed flame, as presented by Pack et al. [12]. This calibration was performed with a mask on the primary detection lens to avoid biasing from fluorescence vignetting, although the SBR in the jet flame is about 2.0 without any mask. This procedure is apparently sufficient for determination of the concentration within $\sim 10\%$ at the sampling rates required for turbulent flames, although even better measurements could be obtained if the flame emission background were reduced further.

4 Conclusions

A saturation-correction scheme was derived for application to gated photon counting measurements. This routine was shown to yield the same fluorescence lifetimes for liquid samples of diphenyloxazole and quinine sulfate monohydrate as those from previous unsaturated measurements by Pack et al. [11]. The technique was then extended to hydroxyl measurements at a sampling rate of 1–100 Hz in laminar premixed, laminar counterflow diffusion, and laminar jet diffusion flames. In each case, the results match either previous LSF measurements or LIFTIME measurements taken at low photon count rates. Thus, we have shown that the saturate-and-compare algorithm is sufficiently robust for applications to a wide range of practical flames at a wide range of signal levels and SBRs.

Measurements in the laminar jet diffusion flame were further extended to a sampling rate of 4 kHz and were found to agree with measurements at a lower sampling rate while displaying an uncertainty of $\sim 10\%$. For application to turbulent flames, this sampling rate is sufficient for detailed study of the power spectral density [10]. Moreover, the uncertainty in concentration is even less than that for instrumentation noise from our previous fluorescence time-series measurements. Hence, the gated, photon-counting system is sufficient for detailed time-series measurements. Future measurements in turbulent flames should provide for the first time quantitative, quenching-independent minor-species concentration time series. Such measurements can be compared to our previous fluorescence measurements [9, 10] so as to examine the importance of quenching corrections for accurate time-series measurements.

Appendix A. Saturate-and-compare: derivation and implementation

A.1 Saturate-and-compare derivation

An array representing a perfect fluorescence decay was constructed from the assumed decay parameters as

$$F_i = A \exp\left(\frac{-t_i}{\tau}\right) + B\,, \tag{A.1}$$

where F_i is the average value of the exponential decay (photoelectrons/second) at time t_i for a single laser pulse and A is the peak decay amplitude at $t = 0$ (just following the laser pulse). The numerical time step, $\delta t = t_{i+1} - t_i$, was chosen to be 100 ps, thus providing 125 points in a decay array of 12.5 ns total duration (the period of the 80 MHz laser).

The decay array was saturated by assuming Poisson distributed photon counts and a fixed value of the system DPR. Thus, the probability of receiving no counts from the PMT in a specified period of time is $\exp(-\mu)$, where μ is the average number of counts. The probability of the discriminator not being dead for the i^{th} time bin, ND_i, is related to the probability of measuring no photons in the previous DPR, and is computed as

$$ND_i = \prod_{j=i-dpr}^{i-1} \exp(-M_j) \approx \exp\left[-\sum_{j=i-dpr}^{i-1} M_j\right]\,, M_j^2 \ll 1\,, \tag{A.2}$$

where dpr is the number of array points associated with the DPR and M_j is the average number of measured photons at time t_j. Since the decay parameters do not change on the time scale of the laser repetition rate (12.5 ns), the present and previous laser pulses are statistically identical so that negative array points can be computed by use of $M_j = M_{125+j}$. Combining (A.2) with the probability of receiving at least one photon in the i^{th} bin, the probability of measuring a photon during the time period $t_{i-1/2} < t < t_{i+1/2}$ for a single laser pulse is

$$M_i = \left\{\exp\left[-\sum_{j=i-dpr}^{i-1} M_j\right]\right\}\{1 - \exp(-F_i \delta t)\}\,. \tag{A.3}$$

The dual interpretation of M_i as both a probability and a photoelectron count is permitted since M_i is a very small number so that the probability of measuring at least one photoelectron is $1 - \exp(-M_i) \approx M_i$. Since the degree of saturation depends on the previously measured counts, M_i is recursive. Once the first dpr points of the M_i array have been computed, the remaining points can be found explicitly.

An approximate method for computing the first dpr points of M_i was required to avoid a time-consuming iterative solution to (A.3). For typical OH measurements, the last dpr points of the array are mostly background and nearly constant. Thus, the saturation behavior of the final dpr points of the array was estimated from the average count in these channels. These points, $M_i^{(1)}$, were computed as

$$M_i^{(1)} = \left\{\exp\left[-\sum_{j=126-dpr}^{125} F_j \delta t\right]\right\}\{1 - \exp(-F_i \delta t)\}\,,$$
$$i > 125 - dpr\,. \tag{A.4}$$

This array, representing the last dpr points, was then used to compute the entire decay array, $M_i^{(2)}$, explicitly by

$$M_i^{(2)} = \begin{cases} \left\{\exp\left[-\sum_{j=i-dpr+125}^{125} M_j^{(1)} - \sum_{j=1}^{i-1} M_j^{(2)}\right]\right\} \\ \quad \times \{1 - \exp(-F_i \delta t)\}\,, i \le dpr \\ \left\{\exp\left[-\sum_{j=i-dpr}^{i-1} M_j^{(2)}\right]\right\}\{1 - \exp(-F_i \delta t)\}\,, \\ \quad i > dpr\,. \end{cases} \tag{A.5}$$

This approximation scheme was found to be sufficient for the full range of operating conditions of the photon-counting system. Selected measurements were analyzed by iterative solution of (A.3) without the above approximations and yielded nearly identical results as for (A.4) and (A.5).

A.2 Saturate-and-compare implementation

After computing the saturated decay, $M_i^{(2)}$, the estimated photoelectron counts for the four bins (D_1–D_4) were calculated by summation over the number of laser pulses for the appropriate portions of the decay (while accounting for any temporal delay, t_o, between bin D_2 and the laser pulse). The numerically updated guesses for A, B, and τ were computed from simple ratios of measured to computed bin counts. A damping coefficient, $d = 0.8$, was included for numerical stability. The initial guesses, A^0, B^0, and τ^0 were determined from the unsaturated expressions, (1)–(4) used previously by Pack et al. [11]. This scheme decreased the number of iterations required and also ensured that the correct values were recovered in the unsaturated limit. As photon saturation becomes more significant, these simple expressions can be undefined or provide initial guesses that are too far removed from the correct answer. In these cases, the initial lifetime was assumed to be 1.0 ns.

The convergence criterion for the above algorithm was based on the error in the i^{th} iteration and was computed via

$$E_i = \sum_{j=2,3,4} \left| \frac{D_j^m - D_j^i}{D_j^i} \right| . \qquad \text{(A.6)}$$

Note that this fractional error does not include bin D_1 since secondary saturation at the pulse counting boards is not included in the model. New values of A, B, and τ were computed until E_i was less than 0.1% or until 100 iterations had been performed. The 0.1% error is smaller than the uncertainty (95% confidence interval) in the measured bins from shot-noise alone for most of our measurements, and was typically achievable within 5–20 iterations of the saturation routine. Lack of convergence occurred only in regions where there was little or no OH concentration (such as in the air or the pure-fuel streams when performing radial profiles in a diffusion flame). For the present data, this timeout was only significant when the OH concentration was less than about 5% of its peak value. Above this concentration every data point of the hydroxyl time-series converged for the signal-to-background ratios and signal levels reported in this investigation.

In general, the saturate-and-compare algorithm required about 2–5 min for analysis of each 4096-point time series (on a 200-MHz PC with 32-MB of RAM). To facilitate faster data collection, the time series were stored and a batch file was constructed as the data were collected. The raw time-series files expressed as bin counts were then converted to time series of fluorescence lifetime and concentration overnight. The saturate-and-compare code is available via the Internet for both FORTRAN and LabVIEW® [21].

Appendix B. Saturate-and-compare: calibration

Measurements of diphenyloxazole (PPO) fluorescence were analyzed while varying the values of DPR and t_o in the model. The PPO was excited at 309 nm and fluorescence was detected in a 10-nm window centered at 440 nm. For approximately half of the measurements a flashlight was placed behind the PPO cuvette to simulate flame emission background. By adjusting the angle of the flashlight and the monochromator entrance slit, we were able to vary the range of signal levels and signal-to-background ratios (SBRs). Thirty-three measurements were considered with absolute signal levels ranging from $\sim$ 6 million to $\sim$ 34 million photoelectrons/second and with SBRs ranging from 0.19 to 4.56. The 33 PPO measurements were analyzed for many numerical combinations of DPR and t_o, and a range of lifetimes was computed ($\tau_{max} - \tau_{min}$) for each combination. The smallest lifetime error was found for a DPR of 6.5 ns and an initial delay of 0.9 ns. At this point the range of lifetimes was 0.037 ns. The average value of the lifetime found using these values (1.27 ns) was consistent with that determined by Pack et al. [11] when employing a low photon count and an established convolute-and-compare algorithm. Furthermore, these parameters were found to be consistent with other direct measurements of DPR and t_o for our photon-counting system. Further details of the saturation correction are available with the FORTRAN code [21].

Acknowledgements. This work was supported by the Air Force Office of Scientific Research, with Dr. J. Tishkoff as technical monitor and by the Department of Defense NDSEG Fellowship Program (M. Renfro).

References

1. H. Tennekes, J.L. Lumley: *A First Course in Turbulence* (MIT Press, Cambridge, MA 1972)
2. L. Mydlarski, Z. Warhaft: J. Fluid Mech. **320**, 331 (1996)
3. I. Gökalp, I.G. Shepherd, R.K. Cheng: Combust. Flame **71**, 313 (1988)
4. J.D. Li, R.J. Brown, R.W. Bilger: *Turbulent Shear Flws* 9 (Springer, Berlin, Heidelberg 1983) p. 411
5. S.M. Masutani, C.T. Bowman: J. Fluid Mech. **172**, 93 (1986)
6. M.Q. McQuay, S.M. Cannon: Combust. Sci. and Technol. **119**, 13 (1996)
7. M.E. Kounalakis, J.P. Gore, G.M. Faeth: Twenty-second Symposium (International) on Combustion (The Combustion Institute 1988) p. 1281
8. R.W. Dibble, R.E. Hollenbach: Eighteenth Symposium (International) on Combustion (The Combustion Institute 1981) p. 1489
9. M.W. Renfro, M.S. Klassen, G.B. King, N.M. Laurendeau: Opt. Lett. **22**, 175 (1997)
10. M.W. Renfro, S.D. Pack, G.B. King, N.M. Laurendeau: Combust. Flame **115**, 443 (1998)
11. S.D. Pack, M.W. Renfro, G.B. King, N.M. Laurendeau: Opt. Lett. **23**, 1215 (1998)
12. S.D. Pack, M.W. Renfro, G.B. King, N.M. Laurendeau: Combust. Sci. and Technol. **140**, 405 (1999)
13. P.B. Coates: J. Phys. E **1**, 878 (1968)
14. P.B. Coates: J. Phys. E **5**, 148 (1972)
15. D.E. Donohue, R.C. Stern: Rev. Sci. Instrum. **43**, 791 (1972)
16. D.V. O'Connor, D. Phillips: *Time-correlated Single Photon Counting.* (Academic Press, London 1984)
17. A.J. Alfano, F.K. Fong, F.E. Lytle: Rev. Sci. Instrum. **54**, 967 (1983)
18. A.J. Alfano: Appl. Opt. **28**, 5010 (1989)
19. S.D. Pack: M.S. Thesis, Purdue University, West Lafayette, IN 1998

20. J.B. Atkinson: J. Phys. E **10**, 482 (1977)
21. Flame Diagnostics Laboratory, Purdue University: http://widget.ecn.purdue.edu/∼flames/ (1998)
22. R.A. Lampert, L.A. Chewter, D. Phillips, D.V. O'Connor, A.J. Roberts, S.R. Meech: Anal. Chem **55**, 68 (1983)
23. R.F. Chen: Anal. Biochem. **57**, 593 (1974)
24. M.S. Klassen, B.D. Thompson, T.A. Reichardt, G.B. King, N.M. Laurendeau: Combust. Sci. and Technol. **97**, 391 (1994)
25. J.R. Reisel, C.D. Carter, N.M. Laurendeau: Energy and Fuels **11**, 1092 (1997)
26. R.J. Kee, J.F. Grcar, M.D. Smooke, J.A. Miller: Sandia Report SAND85-8240, Sandia National Laboratories. Livermore, CA (1985)
27. C.T. Bowman, R.K. Hanson, D.F. Davidson, W.C. Gardiner Jr., V. Lissianski, G.P. Smith, D.M. Golden, M. Frenklach, M. Goldenberg: http://www.me.berkeley.edu/gri_mech/ (1995)
28. R.V. Ravikrishna, N.M. Laurendeau: Combust. Flame **113**, 473 (1998)